Atomic dynamics with photon-dressed core states

F. Robicheaux
Department of Physics and The Joint Institute for Laboratory Astrophysics, University of Colorado, Boulder, Colorado 80309-0440
(Received 14 September 1992)

This paper describes the atomic dynamics when a Rydberg atom is in a laser field which is resonant with a dipole-allowed core transition. The main approximation is to *completely* ignore the (short-range, direct) interaction of the outer electron with the resonant laser which is the same approximation used with great success in calculating the spectrum due to isolated core excitations (ICE). The atom autoionizes when the core absorbs a photon, because the electron can then inelastically scatter from the excited core state, gaining enough energy to escape the atom. Despite neglecting the direct interaction between the outermost electron and the laser, the laser profoundly affects the autoionization dynamics. This effect is incorporated through a frame transformation between the dressed and undressed core states which only utilizes the field free atomic scattering parameters. A two-color experiment is proposed which might be able to measure nonperturbative effects arising from the dressed core states. The usual ICE transition rate is obtained through a perturbative expansion. Generic effects are examined through a model problem. A calculation of the Mg spectrum when the driving laser is tuned to the $3s_{1/2}$-$3p_{1/2}$ or the $3s_{1/2}$-$3p_{3/2}$ transition is presented.

PACS number(s): 32.80.Rm, 32.80.Dz, 32.80.Fb, 32.80.Wr

I. INTRODUCTION

The description of nonperturbative atom-light interactions is an intractable problem at this point for all but the simplest atoms and ions [1,2]. In this paper, we describe a class of interactions which seems to be amenable to a nearly exact treatment. The dynamics is similar in spirit to that in isolated core excitations [3] (ICE) where a Rydberg atom is immersed in light which is nearly resonant with a dipole-allowed core transition. The Rydberg electron hardly interacts with the light because it spends most of its time at very large distances from the nucleus where it only feels a very small force. The calculated ionization rates due to isolated core excitations are in very good agreement with experiment; the theoretical rates are obtained by *completely* ignoring the amplitude for direct excitation of the outer electron into the continuum.

The effects seen in ICE experiments are perturbative; we propose examining the nonperturbative regime where the Rabi oscillation of the dressed core states is nearly equal to or faster than the classical Rydberg frequency of the outer electron. In the language of multichannel quantum-defect theory (MQDT) [4], we will describe the atomic dynamics (autoionization, etc.) of dressed channels. An experiment which might show these effects would bathe atoms with a strong laser near a transition frequency of the positive ion; this laser has practically no effect on the low atomic states since it is not resonant with any atomic transition. A weak probe laser can be scanned in the region near the *atomic* thresholds (the ionic core states are resonant with the strong laser once the electron excited by the probe laser is farther than ~ 20 a.u. from the nucleus). The ionization rate will show nonperturbative effects due to the dressed core states when the Rabi frequency d_{12} is nearly equal to or larger than the classical orbital frequency $1/n^{*3}$ of the outer Rydberg electron, i.e., $d_{12}n^{*3} \geq 1$.

The motivation for studying the dynamics of a Rydberg atom with dressed core states is similar to the motivation for studying atomic dynamics in static fields [5]. The external field breaks the rotational symmetry of the atom and forces the electron to explore larger regions of phase space. The resulting dynamics is much richer that the unperturbed atomic dynamics. Unlike the static electric and magnetic fields which dominate the Coulomb field at large distances, the laser field only breaks the symmetry near the nucleus; it does not change the long-range forces felt by the electron [6]. The number of channels needed to describe the interaction of an electron with dressed core states is much less than that needed to describe Rydberg electrons in static electric or magnetic fields which makes the theory more tractable. In a sense, this work is also related to the studies of atom-atom scattering in laser fields [7]; the detailed dynamics depends on the atom, but some important processes which can be easily interpreted do not depend on the specific atom.

In Sec. II we give a brief description of dressed states in a classical laser field in the rotating-wave approximation. In Sec. III we describe in detail the atomic dynamics with dressed core states, discussing our approximation and the range of its validity. In Sec. IV, we discuss the perturbative limit of the dressed core dynamics; we show how to obtain the isolated core excitation results and the frequency range over which the perturbative limit is valid. In Sec. V, we discuss a simple model problem which should illustrate the dynamics. In Sec. VI we apply the formalism of Sec. III to Mg with the strong laser driving either the $3s_{1/2}$-$3p_{1/2}$ or the $3s_{1/2}$-$3p_{3/2}$ transitions. The atomic case is more subtle than the model described in Sec. V due to the coupling of the core angular momentum to that of the outer electron. We conclude with Sec. VII.

II. DRESSED STATES IN THE FLOQUET REPRESENTATION

In this section, we show how to obtain the dressed states from the Floquet representation within the rotating-wave approximation. This procedure for obtaining the dressed states is well known; we go into the details here so that various parameters used in the later sections have specific definitions. We will always use classical oscillating fields to drive the core states; we ignore spontaneous emission from the dressed states which will be a good approximation as long as the Rydberg electrons autoionize faster than the natural lifetime of the core states (and as long as the Rabi frequency is much greater than the spontaneous decay rate).

The Hamiltonian for two states being driven by a classical laser field is

$$H=|1\rangle E_1\langle 1|+|2\rangle E_2\langle 2|+|1\rangle d_{12}\cos\omega t\langle 2| +|2\rangle d_{21}\cos\omega t\langle 1|, \tag{1}$$

where (we assume) $E_2>E_1$ and $d_{12}=\langle 1|\mathbf{F}\cdot\mathbf{r}|2\rangle=d_{21}$. There are two linearly independent solutions of the equation $(i\partial/\partial t)|\phi_\alpha(t)\rangle=H|\phi_\alpha(t)\rangle$, which have a quasi-time-independent form. We expand $|\phi_\alpha(t)\rangle$ in terms of states $|1\rangle$ and $|2\rangle$ with time-dependent coefficients,

$$|\phi_\alpha(t)\rangle=\exp(-i\bar{E}_\alpha t)(|1\rangle\bar{U}_{1\alpha}+\exp(-i\omega t)|2\rangle\bar{U}_{2\alpha}), \tag{2}$$

where the $\bar{U}$ and $\bar{E}$ are constants. We now make the rotating-wave approximation to obtain an eigenvalue matrix equation for $\bar{E}_\alpha$ and $\bar{U}_{i\alpha}$. This equation is

$$\begin{bmatrix} E_1 & d_{12}/2 \\ d_{21}/2 & E_2-\omega \end{bmatrix}\begin{bmatrix}\bar{U}_{1\alpha}\\ \bar{U}_{2\alpha}\end{bmatrix}=\begin{bmatrix}\bar{U}_{1\alpha}\\ \bar{U}_{2\alpha}\end{bmatrix}\bar{E}_\alpha. \tag{3}$$

For the experiments we are interested in, we do not think it is presently possible to obtain $|d_{12}|>10^{-5}$ a.u., and the rotating-wave approximation should thus work very well. The eigenvectors $\bar{U}$ are unitary, i.e., $\bar{U}^\dagger\bar{U}=\bar{U}\bar{U}^\dagger=1$. The final important point is that Eq. (2) can be "inverted" to obtain states $|1\rangle$ and $|2\rangle$ in terms of the eigenstates, $|\phi_\alpha(t)\rangle$. These formulas are important for the formulation presented in Sec. III and are given by

$$|1\rangle=\sum_\alpha|\phi_\alpha(t)\rangle\exp(i\bar{E}_\alpha t)(\bar{U}^\dagger)_{\alpha 1}, \tag{4a}$$

$$|2\rangle=\sum_\alpha|\phi_\alpha(t)\rangle\exp(i[\bar{E}_\alpha+\omega]t)(\bar{U}^\dagger)_{\alpha 2}. \tag{4b}$$

Equations (1)–(4) can be easily generalized when there are more than two atomic states or laser fields.

III. ATOMIC DYNAMICS WITH DRESSED CORE STATES

A. Proposed experiment and approximations

The basic dynamics of isolated core excitations are very simple [3]. A Rydberg electron orbits a positively charged ion, spending most of its time at very large distances. A laser field (nearly resonant with a dipole-allowed transition between two of the ionic states) interacts with the Rydberg atom causing the atom to ionize. The outer electron does not directly absorb any photons because it spends most of its time at large distances from the nucleus. However, the core electrons can (and do) absorb photons; the outer electron inelastically scatters from the excited core producing an ionization signal. No significant discrepancy between theory and experiment has been detected, even though the interaction between the Rydberg electron and the laser is completely ignored when calculating the rate of ionization. Most importantly, the calculations and experiments agree on differential cross sections which are notoriously sensitive to theoretical errors.

The dynamical situation we are exploring is simply an extension of the isolated core excitations. What we propose to do is to examine the dynamics when the laser which drives the core electrons is strong enough to give a large Rabi splitting to the core states. A new dynamical process occurs when the Rabi oscillations of the core states is nearly equal to or larger than the Rydberg frequency, $1/n^{*3}$, of the outer electron. It is clear that we do not need to directly account for the interaction of the outer electron with the driving laser field for the same reason as in the theory of isolated core excitations; the outer electron only feels the effects of this field through its interaction with the core electrons.

An experiment which should see these effects is easy to visualize but will be very difficult to implement in practice. (i) Pass a "strong" laser field which has its frequency resonant (or nearly resonant) with a transition of a positive ion through the atomic gas. This will be called the *driving* laser field. Because the driving laser is *not* resonant with a bound *atomic* transition, it has no effect on the gas. (ii) While the driving laser is on, pass a weaker probe laser through the same region of the gas; the probe laser having a higher frequency than the driving laser. The probe-laser frequency needs to be high enough to excite the atoms to their threshold region. (iii) Measure the cross section for absorbing a probe-laser photon, or for photoionization, as a function of the probe-laser frequency for given intensity and detuning of the driving laser. Once the probe laser ejects an electron to large distances, the core becomes resonant with the driving laser and starts oscillating between the resonant states with the Rabi oscillation frequency, d_{12}. If the outer electron returns to the core before the states begin to oscillate (i.e., d_{12} is much less than the classical frequency of the outer electron), the dynamics are nearly identical to that with the driving laser off. This is the perturbative case and is identical to the usual ICE experiments; we discuss this limit in Sec. IV. If the electron returns to the core on the scale of the period of the Rabi oscillations ($d_{12}\sim 1/n^{*3}$), the dynamic of the core and outer electron becomes strongly entangled; the resulting dynamics is thus completely changed from field-free atomic dynamics. As seen in Secs. V and VI there are some regions near $n^*\sim d_{1/2}^{1/3}$ where spectra will appear to be simple. When the core oscillates many times before the electron returns, the dynamics again decouples and we see simple Rydberg series

attached to thresholds given by the Floquet quasienergy of the dressed core states.

The difficulty with real experiments lies with the necessity of achieving a strong enough driving field. The strength of the driving field needed to see the nonperturbative effects is directly related to the resolution of the weak probe laser. The resolution of the probe laser determines how high in n^* the atomic states can be resolved and thus the size of d_{12} needed to find nonperturbative effects. Basically, nonperturbative effects will be observed if the frequency of the Rabi oscillations induced by the driving laser is larger than the resolution of the probe laser. Note that we were vague about which core transitions need to be driven. In fact, *any* allowed transition in which one of the terms is part of an important channel in the undressed atomic dynamics will suffice. This includes downward transitions, transitions between two excited ionic states, as well as upward transitions. For example, in Ca the driving laser can be tuned to the $4s_{1/2}$-$4p_J$ transitions, or the $3d_J$-$4p_{J'}$ transitions, or the $3d_J$-$4f_{J'}$ transitions.

Before introducing the formalism which we will use to describe this problem, we will discuss the suitability as well as the range of applicability of the main approximation contained in our method. This approximation consists of completely ignoring the direct effect of the driving field on the Rydberg electron. The interaction we are ignoring is what causes above-threshold ionization (ATI) in one-electron atoms. So our method completely breaks down when the driving laser field is strong enough to give substantial above threshold ionization. For optical fields, we expect our approximations to hold for field strengths less than $\sim 10^{11}$ W/cm^2 $\sim 10^{-6}$ a.u. The Rabi frequency goes like the square root of the field strength, when the driving frequency is exactly on resonance. Assuming the probe laser can resolve Rydberg states near $n=35$ gives a minimum field strength (needed to see nonperturbative effects) of $\sim 10^{-11}$ a.u., five orders of magnitude smaller than the fields for which the approximation breaks down. For infrared fields, the field strength for substantial ATI is smaller but there is still a large range of acceptable field strengths. Of course, our method fails completely for driving fields in the microwave regime.

B. Formalism

We now introduce the tools to describe the dynamical problem through a model problem. In Sec. VI we discuss a real atomic problem and introduce at that point some extra features which are not described in this section.

Our model is the simplest that will still show these dynamical effects. In this model problem, the core (ionic) state $|1\rangle$ of Sec. II will be an s state $|S\rangle$, and the core state $|2\rangle$ will be a p state $|P\rangle$; the energy of the s state is lower than that of the p state. The outer Rydberg electron can be either an s wave or a p wave. The driving laser has a frequency ω_d near the s-p transition of the ion, $E_p - E_s$. The probe laser has a frequency ω_p which is near the transition from the ground state (which is assumed to have even parity) to the lower threshold of the ionic state $|S\rangle$. In this energy range the channel attached to the core $|P\rangle$ is assumed to be strongly closed and thus the wave function excited by the probe laser (in the absence of the driving laser) is

$$\psi_s^{(0)} = e^{-iEt}\{|S\rangle Y_1[f_{\varepsilon_s^{(0)},1}(r) - g_{\varepsilon_s^{(0)},1}(r)K_{ss}^{(0)}(E)]\}, \quad r > r_c, \tag{5}$$

where we have explicitly written the time dependence $\exp(-iEt)$, Y_1 is the spherical harmonic of the outer electron, r_c is the size of the core state, $f_{\varepsilon_s^{(0)},1}$ ($g_{\varepsilon_s^{(0)},1}$) is the regular (irregular) Coulomb function of angular momentum $l=1$ and energy $\varepsilon_s^{(0)} = E_g + \omega_p - E_s$, and $K_{ss}^{(0)}(E)$ is the reaction matrix at energy E which is $\tan\pi\mu_s(E)$ in this simple one-channel problem. The only other dynamical parameter of interest is the reduced dipole matrix element $d_s^{(0)}$, which connects the ground state to the excited state of Eq. (5).

The driving laser field will connect the wave function of Eq. (5) to those of opposite parity and higher in energy by ω_d; the driving laser causes a mixing between the wave function of Eq. (5) and the next higher Floquet mode. At this energy $E+\omega_d$, both channels are open and weakly closed. There are two linearly independent solutions of the field-free Schrödinger's equation of even parity and energy $E+\omega_d$ given by

$$\psi_s^{(+)} = e^{-i(E+\omega_d)t}\{|S\rangle Y_0[f_{\varepsilon_s^{(+)},0} - g_{\varepsilon_s^{(+)},0}K_{ss}^{(+)}(E+\omega_d)] - |P\rangle Y_1 g_{\varepsilon_p^{(+)},1}K_{ps}^{(+)}(E+\omega_d)\}, \tag{6a}$$

$$\psi_p^{(+)} = e^{-i(E+\omega_d)t}\{|P\rangle Y_0[f_{\varepsilon_p^{(+)},1} - g_{\varepsilon_p^{(+)},1}K_{pp}^{(+)}(E+\omega_d)] - |S\rangle Y_0 g_{\varepsilon_s^{(+)},0}K_{sp}^{(+)}(E+\omega_d)\}, \tag{6b}$$

where $\varepsilon_{s,p}^{(+)} = E_g + \omega_p - E_{s,p} + \omega_d$ and $\underline{K}^{(+)}$ is the reaction matrix at energy $E+\omega_d$ for the states of even parity. The most important point is that the wave functions of Eqs. (5) and (6) are slowly varying in energy at small radii [4] because (as is usual in MQDT) we have not imposed the boundary conditions at $r \to \infty$. Equations (5) and (6) contain exponentially diverging pieces if any of the channels are closed. When the driving field is off, these wave functions are *exact* solutions of the time-dependent Schrödinger equation for the atom.

We now obtain the three linearly independent solutions, when the outer electron is at distances $r > r_c$, which satisfy the full time-dependent Schrödinger equation with the driving field on. They are

$$\bar{\psi}_1(t)=e^{-iEt}\left[\sum_{j=1}^{2}|\phi_j(t)\rangle Y_1(f_{\varepsilon_j,1}\delta_{j1}-g_{\varepsilon_j,1}\bar{K}_{j1})-|S\rangle e^{-i\omega_d t}Y_0 g_{\varepsilon_s^{(+)},0}\bar{K}_{s1}\right], \tag{7a}$$

$$\bar{\psi}_2(t)=e^{-iEt}\left[\sum_{j=1}^{2}|\phi_j(t)\rangle Y_1(f_{\varepsilon_j,1}\delta_{j2}-g_{\varepsilon_j,1}\bar{K}_{j2})-|S\rangle e^{-i\omega_d t}Y_0 g_{\varepsilon_s^{(+)},0}\bar{K}_{s2}\right], \tag{7b}$$

$$\bar{\psi}_s(t)=e^{-iEt}\left[|S\rangle e^{-i\omega_d t}Y_0(f_{\varepsilon_s^{(+)},0}-g_{\varepsilon_s^{(+)},0}\bar{K}_{ss})\sum_{j=1}^{2}|\phi_j(t)\rangle Y_1 g_{\varepsilon_j,1}\bar{K}_{js}\right], \tag{7c}$$

where $\varepsilon_\alpha=E_g+\omega_p-\bar{E}_\alpha$. Equations (7) are exact solutions of the full time-dependent Schrödinger equation for $r>r_c$ when we ignore the direct coupling of the driving laser field to the outer electron. The purpose of this paper is to show how it is possible to obtain the $\bar{K}$ matrix of scattering parameters from the scattering parameters of the wave functions of Eqs. (5) and (6) which are solutions of the time-dependent Schrödinger's equation with the driving laser off.

Actually, the term $\exp[-i(E+\omega_d)t]|S\rangle Y_0 g_{\varepsilon_s^{(+)},0}$ in all three solutions is not an exact solution of the time-dependent Schrödinger equation. It should be mixed with the state $\exp[-i(E+2\omega_d)t]|P\rangle Y_0 g_{\varepsilon_p^{(2+)},0}$. However, this mixing has no measurable effect since this channel is open. In MQDT, a frame transformation (which is all that our theory amounts to) that only mixes open channels has no effect on the total cross section; it only mixes the partial cross sections. If we were to take into account this mixing, instead of having an outward flux F of electrons with energy $\varepsilon_s^{(+)}$ we would have a flux $F|\bar{U}_{s1}|^2$ with energy $\varepsilon_s^{(+)}+E_s-\bar{E}_1$ and a flux $F|\bar{U}_{s2}|^2$ with energy $\varepsilon_s^{(+)}+E_s-\bar{E}_2$. The Rabi splitting would need to be $\sim 10^{-4}$ a.u. before this energy difference would be detectable.

When the driving field is turned on, the solutions (5) and (6) become mixed. To determine how to accomplish this mixture we will examine the solutions at $r\sim r_c$. We first make two linearly independent solutions in the place of $\psi_s^{(0)}$ and $\psi_p^{(+)}$ by superposing them

$$\psi_\alpha=\psi_s^{(0)}\bar{U}_{s\alpha}+\psi_p^{(+)}\bar{U}_{p\alpha}, \tag{8a}$$

where $\alpha=1$ and 2 and

$$\psi_3=\psi_s^{(+)}. \tag{8b}$$

The ψ_α's are exact solutions of the time-dependent Schrödinger's equation with the driving field off. We assume that the driving field is nearly resonant with the s-p transition of the core (i.e., $\omega_d\simeq E_p-E_s$) which means $\varepsilon_p^{(+)}\cong\varepsilon_s^{(0)}$. (Furthermore, since we are at small radii $f_{\varepsilon_s^{(0)},1}\cong f_{\varepsilon_p^{(+)},1}$ and $g_{\varepsilon_s^{(0)},1}\cong g_{\varepsilon_p^{(+)},1}$). Now substitute the expression for $|S\rangle$ of Eq. (4a) into Eq. (5) and the expression for $|P\rangle$ of Eq. (4b) into Eqs. (6). If we now use the fact that $f_{\varepsilon_\alpha}\cong f_{\varepsilon_s^{(0)}}\simeq f_{\varepsilon_p^{(+)}}$ at $r\cong r_c$ (and similarly for g), we can obtain the $\bar{K}$ matrix from $K^{(+)}$ and $K^{(0)}$ using simple algebra. This step is the heart of our approximate procedure since the time-dependent wave functions of Eq. (8) are *not* exact solutions to the full time-dependent Schrödinger's equation. The error in the $\bar{K}$ matrix is due to the neglect of the interaction of the atom with the driving laser when *all* of the electrons are at distances $r<r_c$. However, when all of the electrons are at small distances the driving laser is not in resonance because the core states are strongly perturbed by the extra electron. The error in our approximate $\bar{K}$ matrix is of the size of d_{12}. For the reasons mentioned in Sec. III A we do not expect our approximations to work for $|d_{12}|>10^{-3}$; the errors in $\bar{K}$ probably have a negligible effect on the cross section for $|d_{12}|<10^{-3}$. In Ba, the LS to jj frame transformation (which ignores the spin-orbit interaction when all of the electrons are at distances $r<r_c$) works very well even though the fine-structure splitting of the $6p$ thresholds is $\sim 8\times 10^{-3}$ a.u.

In MQDT, the transformation of the solutions (5) and (6) to the exact solutions (7) is called a frame transformation [8]. The transformation matrix [if the solutions are ordered $\psi_1=\psi_s^{(0)}$, $\psi_2=\psi_s^{(+)}$, and $\psi_3=\psi_p^{(+)}$ and $\bar{\psi}_3=\bar{\psi}_s^{(+)}$],

$$\underline{U}=\begin{bmatrix}\bar{U}_{s1} & \bar{U}_{s2} & 0\\ 0 & 0 & 1\\ \bar{U}_{p1} & \bar{U}_{p2} & 0\end{bmatrix}, \tag{9}$$

takes the atomic solutions in the absence of an interaction to the exact solutions,

$$\bar{\psi}_\alpha=\sum_i \psi_i U_{i\alpha}. \tag{10}$$

Furthermore, all of the exact dynamical parameters are obtained by a transformation of the field-free dynamical parameters. The exact reaction matrix and dipole matrix elements are

$$\underline{\bar{K}}=\underline{U}^{\dagger}\underline{K}\,\underline{U}, \tag{11}$$

$$\bar{d}=d\underline{U}. \tag{12}$$

All of the barred parameters refer to the states with the driving laser on; however, they are not the physical parameters because the barred wave functions diverge exponentially in all of the closed channels when propagated to large distances.

In the discussion above it was easier to use real wave functions and scattering parameters, $\underline{K}$ and $\bar{d}$. However, in Secs. IV and V it is easier to understand some of the dynamics using the S matrix and complex dipole matrix elements. It is very easy to obtain one set of scattering parameters [4] in terms of the other set. The scattering matrix can be easily found in terms of the reaction matrix using

$$\underline{S}=\frac{1+i\underline{K}}{1-i\underline{K}}. \tag{13}$$

The analog of Eq. (11) for the S matrix is

$$\bar{\underline{S}}=\underline{U}^{\dagger}\underline{S}\,\underline{U}=\frac{1+i\bar{\underline{K}}}{1-i\bar{\underline{K}}}. \tag{14}$$

The wave function which has purely incoming waves in all of its channels except the α'th can be found in terms of the wave function with standing-wave boundary conditions as

$$\bar{\Psi}_{\alpha'}=\sum_{\alpha}\bar{\psi}_{\alpha}[(1-i\bar{\underline{K}})^{-1}]_{\alpha\alpha'}. \tag{15}$$

The dipole matrix elements which connect the ground state to the states $\bar{\Psi}$ are

$$\bar{D}=\bar{d}(1-i\bar{\underline{K}})^{-1}=D\underline{U}, \tag{16}$$

where

$$D=d(1-i\underline{K})^{-1}. \tag{17}$$

All of the barred parameters refer to the dynamical parameters with the driving laser on; the unbarred parameters are for the states with the driving laser off.

To obtain the cross section we need to superpose the $\bar{\Psi}_{\alpha}$ to obtain the correct boundary conditions at $r\to\infty$. These conditions are that the wave function must converge to zero in the closed channels and obey incoming wave boundary conditions in the open channels. For the case when channels 1 and 2 are closed and channel 3 is open, these conditions are satisfied by the wave function [4]

$$\bar{\Psi}_f=\bar{\Psi}_3-(\bar{\Psi}_1\,\bar{\Psi}_2)\begin{pmatrix}\bar{S}_{11}-e^{-2i\pi\nu_1} & \bar{S}_{12}\\ \bar{S}_{21} & \bar{S}_{22}-e^{-2i\pi\nu_2}\end{pmatrix}^{-1}\times\begin{pmatrix}\bar{S}_{13}\\ \bar{S}_{23}\end{pmatrix}, \tag{18}$$

where $\nu_j=1/\sqrt{2(\bar{E}_j-E)}$ is the effective quantum number of channel j which is also written as n_j^*. The dipole matrix element which connects this state to the ground state is

$$\bar{D}_f=\bar{D}_3-(\bar{D}_1\,\bar{D}_2)\begin{pmatrix}\bar{S}_{11}-e^{-2i\pi\nu_1} & \bar{S}_{12}\\ \bar{S}_{21} & \bar{S}_{22}-e^{-2i\pi\nu_2}\end{pmatrix}^{-1}\times\begin{pmatrix}\bar{S}_{13}\\ \bar{S}_{23}\end{pmatrix}. \tag{19}$$

When there are closed channels imposing the boundary conditions at $r\to\infty$ introduces rapid energy dependences and causes the appearance of the autoionizing Rydberg series in the cross section.

IV. PERTURBATIVE LIMITS

In this section we describe the perturbative limit, $d_{12}\to 0$. In Sec. IV A we show where the perturbative limit fails as n^* increases for a fixed d_{12}. In Sec. IV B we show how our formalism reproduces the usual ICE results when $d_{12}\ll|E_1+\omega_d-E_2|$ where these parameters are identical to those in Eq. (3). For this discussion we will use the simple three-channel model of Sec. III to facilitate the derivations in Secs. IV A and IV B of this section. The results we derive below are valid for more complicated problems as could be easily shown. In all of what follows we will be in the frequency range where both channels 1 and 2 are closed.

A. Perturbatively split thresholds

In this section we are trying to determine the smallest n^* for which a perturbative treatment breaks down. It is clear that the most effective mixing occurs when $\omega_d=E_2-E_1$ (i.e., the driving laser is exactly on resonance); we will only focus on this situation. To see the perturbative limit most clearly we substitute Eqs. (15) and (16) for the barred values of Eq. (19) to obtain

$$D_f=D\bar{U}(\bar{U}^{\dagger}S_{cc}\bar{U}-e^{-2i\pi\nu_c})^{-1}\bar{U}^{\dagger}S_{c3}, \tag{20}$$

where we have used the fact that $D_i=D_s^{(0)}\delta_{i1}$, and $(S_{cc})_{ij}=\delta_{ij}(\delta_{i1}S_{pp}^{(0)}+\delta_{i2}S_{ss}^{(+)})$, $(S_{c3})_i=\delta_{i2}S_{ps}^{(+)}$, and $(e^{-2i\pi\nu_c})_{ij}=\delta_{ij}e^{-2i\pi\nu_j}$. Since $\bar{U}$ is unitary ($\bar{U}^{-1}=\bar{U}^{\dagger}$) we can easily rewrite D_f as

$$D_f=D(S_{cc}-\bar{U}^{\dagger}e^{-2i\pi\nu_c}\bar{U})^{-1}S_{c3}. \tag{21}$$

The threshold splitting will be small since d_{12} is small and therefore for some range of energy $\nu_1\simeq\nu_2$. We use this fact to approximate $(e^{-2i\pi\nu_c})_{jk}\simeq\delta_{jk}e^{-2i\pi\nu}[1-2i\pi(\nu_j-\nu)]$ where $\nu=1/\sqrt{(E-E_1)}=n^*$ is the effective quantum number when $d_{12}=0$. In the perturbative regime $\nu_1-\nu\simeq d_{12}\nu^3/2$ and $\nu_2-\nu\simeq -d_{12}\nu^3/2$. Substituting these results into Eq. (21) we obtain

$$D_f\cong D(S_{cc}-e^{-2i\pi\nu}-i\pi d_{12}\nu^3\sigma_x e^{-2i\pi\nu})^{-1}S_{c3}, \tag{22}$$

where σ_x is the x component of the Pauli spinors. The only "new" term in Eq. (22) (i.e., absent in the field-free limit) is the term proportional to $\pi d_{12}\nu^3$. This means that perturbative limit obtains when $\pi d_{12}\nu^3\ll 1$; conversely we expect nonperturbative effects to start occurring when $d_{12}\nu^3>0.15$. This result confirms our intuition discussed in the Introduction, i.e., new effects appear when the Rabi frequency times the classical orbital period of the outer electron is on the order of one.

B. Isolated core excitations

We expect a perturbative calculation using our formalism to be able to reproduce the spectrum of isolated core excitations since we are essentially making the same approximation as that made in the ICE calculations. However, it is unclear what will be the mechanism (in our approach) that produces the ICE ripples; in the usual ICE calculations they result from the overlap of the radial wave function of the initial state with the radial wave function of the final state after the core has been excited [3,9]. In this section we obtain the ICE results with our method and describe the mechanism which produces these results.

The ICE experiments [3] use a slightly different setup than that described in Sec. III. In these experiments, the frequency of what we call the probe laser is fixed to a transition from the ground state to a bound Rydberg state with $n^* \geq 10$. What we call the driving laser is scanned in a frequency range near the transition between the core states $|1\rangle$ and $|2\rangle$. The experiment measures the ionization rate as a function of the frequency ω_d of the driving laser. In this section, we derive the usual ICE formula for the dipole matrix element for the simple three-channel problem of Sec. III; the extension to more complicated situations is straightforward, but tedious.

The physical dipole matrix element connecting the ground state to the state with the correct boundary conditions is the same as that of Eq. (20). However, now the driving laser is not resonant and it is weak enough so that we can solve Eq. (3) perturbatively in d_{12}. The unitary transformation matrix $\bar{U}$ can be approximated as

$$\bar{U} \simeq \begin{bmatrix} 1 & \gamma \\ -\gamma & 1 \end{bmatrix} \tag{23}$$

to order $\gamma = d_{12}/[2(E_p - E_s - \omega_d)]$. The eigenenergies are $\bar{E}_1 = E_s$ and $\bar{E}_2 = E_p - \omega_d$ to first order in d_{12}. Substituting these approximations into Eq. (20) and only retaining terms up to first order in γ gives

$$D_f \simeq D_s^{(0)}(1 \quad \gamma) \begin{bmatrix} S_{ss}^{(0)} - e^{-2i\pi\nu_s} & \gamma(S_{pp}^{(+)} - S_{ss}^{(0)}) \\ \gamma(S_{pp}^{(+)} - S_{ss}^{(0)}) & S_{pp}^{(+)} - e^{-2i\pi\nu_p} \end{bmatrix}^{-1} \times \begin{bmatrix} -\gamma \\ 1 \end{bmatrix} S_{pp}^{(+)}. \tag{24}$$

We now invert the matrix to order γ and only keep terms in the final result to this order to obtain

$$D_f \simeq D_s^{(0)}[\gamma(e^{-2i\pi\nu_p} - e^{-2i\pi\nu_s})] \times [(S_{pp}^{(+)} - e^{-2i\pi\nu_p})^{-1} S_{ps}^{(+)}] \times (S_{ss}^{(0)} - e^{-2i\pi\nu_s})^{-1}, \tag{25}$$

where

$$\nu_s = 1/\sqrt{2(E_s - E_g - \omega_p)}$$

and

$$\nu_p = 1/\sqrt{2(E_p - E_g - \omega_p - \omega_d)}$$

The first term in brackets is identical (within a phase factor) to the term in the ICE dipole matrix element resulting from the overlap of the outer Rydberg electron's wave function. To see how this works, use

$$\gamma = d_{12}\nu_s^2\nu_p^2/(\nu_s^2 - \nu_p^2)$$

and

$$[\exp(-2i\pi\nu_p) - \exp(-2i\pi\nu_s)] = 2i\exp(-i\pi[\nu_s + \nu_p])\sin(\pi[\nu_s - \nu_p]);$$

compare this result with Eqs. (20b) and (22) of Ref. [3(c)]. This equivalence is amazing because the first factor in D_f does not appear to have anything to do with the overlap of Rydberg wave functions, Eqs. (6). The second term in brackets is the modulation of the physical dipole matrix element which results from closing the p channel in the $(+)$ wave functions. The final term is a constant since ω_p is fixed. The dipole matrix element of Eq. (25) is exactly the ICE dipole matrix element leaving out phase factors and factors which do not depend on the frequency of the driving laser ω_d.

V. MODEL PROBLEM

In this section, we illuminate the workings of the formalism described in Sec. III by choosing specific values for the parameters of Eqs. (3), (5), and (6). In real atoms, there are many more channels and the dynamics induced by the driving laser can become obscured by the complicated dynamics of the undriven atom.

In this section we fix the dynamic parameters of Eqs. (5) and (6) to be $K_{ss}^{(0)} = 1$, $K_{ss}^{(+)} = -0.5$, $K_{ps}^{(+)} = 0.5$, and $K_{pp}^{(+)} = 1.5$. In the absence of the field, $|S_{ps}^{(+)}|^2 = 0.2$ is the width of the $|P\rangle np$ autoionizing state times n^3. Lastly, the threshold energy $E_s - E_g = 0.1$ a.u.

For the first step in examining the dynamics we set the driving frequency equal to the s-p transition and investigate the dynamics as a function of the field strength of the driving laser measured by d_{12}. We assume the ground state has even parity and the probe-laser frequency is slightly less than 0.1 a.u.

In Fig. 1 we examine how the driving laser disturbs a particular bound level, $|S\rangle 30p$, of the $\psi_s^{(0)}$ state. We graph the three important parameters which characterize this disturbance: the induced width of the state, the shift, and the integrated photoabsorption rate. When the driving laser is off, the $|S\rangle 30p$ state is, of course, stable. Once the driving laser is turned on this state can decay by photoabsorption with a subsequent autoionization; the width measures this decay rate. For small d_{12}, the width of this level is proportional to $|d_{12}|^2$ as expected from time-dependent perturbation theory, Fig. 1(a). Near $d_{12} = 2 \times 10^{-6}$, the width stops increasing like $|d_{12}|^2$ and begins to flatten. At this value of d_{12} the parameter $d_{12}n^3 \sim \frac{1}{18}$ which means that the beginnings of nonperturbative effects may be detectable at smaller $d_{12}n^3$ than expected. The shift in the level position also increases in magnitude like $|d_{12}|^2$ for small d_{12}, Fig. 1(b). In Fig. 1(c) we plot the integrated cross section of this line. This quantity is defined to be $\int \sigma(\lambda) d\lambda$ over the line width. This is the quantity which will be measured experimentally if the resolution of the probe laser is great enough to resolve the individual Rydberg levels near this state but not great enough to resolve the width of this state. This quantity is flat for small d_{12} and begins to decrease near the beginning of the nonperturbative regime. It is possible that the beginnings of the nonperturbative effects will be seen with these parameters, but the evolution of these parameters with d_{12} will possibly never be seen because of the finite resolution of the probe laser.

In Fig. 2 we show the cross section for absorption of a

probe photon as a function of the probe-laser frequency for several different values of d_{12}; the driving laser is, again, exactly on resonance. We have assumed that the probe laser has a resolution of 5×10^{-6} a.u. ~1 cm^{-1} full width at half maximum (FWHM). This figure is meant to give an idea of what combination of experimental tools will be necessary to obtain nonperturbative results. The top curve is the cross section when the Rabi frequency is slightly less than the resolution of the probe laser. The series of peaks follows a strict Rydberg progression and is nearly indistinguishable from the cross sections for much smaller values of the Rabi frequency. For $d_{12}=6\times10^{-6}$ a.u., which is slightly larger than the resolution of the probe laser, we can definitely see nonperturbative effects; two Rydberg series are visible near 0.0997 a.u., one going to each of the Rabi-split thresholds. For even larger d_{12} the nonperturbative effects become more easily visible. This figure shows that the ionization signal as a function of the probe-laser frequency will appear to be identical to that calculated by perturbation theory unless the Rabi frequency is nearly equal to or greater than the resolution of the probe laser.

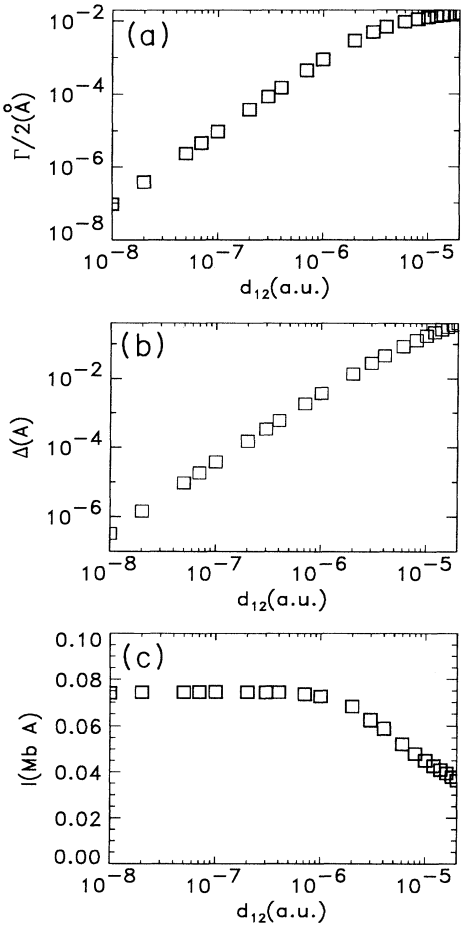

FIG. 1. Parameters which characterize a particular state as a function of d_{12} when the driving laser is exactly on resonance. (a) Width in angstroms of the $|S\rangle30p$ model state. (b) Shift in angstroms of the $|S\rangle30p$ model state. (c) Integrated cross section of the $|S\rangle30p$ model state.

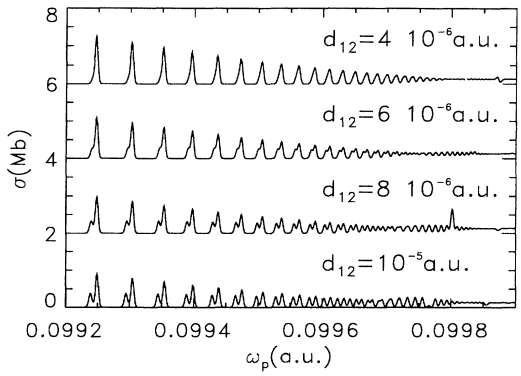

FIG. 2. Cross section for absorption of a probe photon as a function of its frequency, ω_p, for several values of d_{12}. The driving laser is exactly on resonance. The resolution of the probe laser is taken to be 5×10^{-6} a.u.

Another interesting feature of Fig. 2 is the appearance of theoretical deviations in three out of four of the curves. They are at $\sim0.099\,88$ a.u. in the top curve, at ~0.0998 a.u. in the $d_{12}=8\times10^{-6}$ curve, and at $\sim0.099\,76$ a.u. in the bottom curve. These are the energies where $d_{12}=1/n^3$. The reason for these glitches is that there is a state with an *extremely* small width at these energies [10]. To calculate the convoluted cross section, we find the theoretical cross section at 60 000 energy mesh points between 0.099 and 0.1 a.u. We then numerically integrate the theoretical cross section with a Gaussian weight function to obtain the convoluted cross section at ~1200 energy mesh points. Spurious results are obtained when the theoretical width of a resonance is smaller than or equal to the energy mesh. These glitches are artifacts of the finite theoretical mesh which will not appear in an experimental spectrum.

It should not be surprising that the autoionizing width is extremely small when $d_{12}=1/n^3$. At this energy, the classical electron frequency is identical to the Rabi frequency. In other words, the time it takes the electron to return to the nucleus is exactly the same as the time it takes the driving laser to excite and deexcite the core. In this case the electron cannot gain energy by inelastically scattering from the core and therefore it cannot ionize. From Eq. (21) it is fairly easy to show where the zero width states should be or, conversely, what are the values of d_{12} and ω_d which produce zero width states. When $\nu_1=\nu_2+$integer, the matrix $[\exp(-2i\pi\nu_c)]_{ij}=\delta_{ij}\exp(-2i\pi\nu_1)$. Since the identity matrix commutes with all matrices, Eq. (21) reduces to

$$D_f=D(S_{cc}-e^{-2i\pi\nu_1})^{-1}S_{c3}. \tag{26}$$

There is no coupling between channel $|S\rangle$ and $|P\rangle\exp(-i\omega_d t)$ and hence the resonances in $|S\rangle$ cannot decay because d_f now has the same form as when there is *no* driving laser. The resonances are at an energy such that $\nu_1=n-\mu_s^{(0)}$. We have two parameters which characterize the driving laser, d_{12} and ω_d; we can always adjust these two parameters to produce a zero width res-

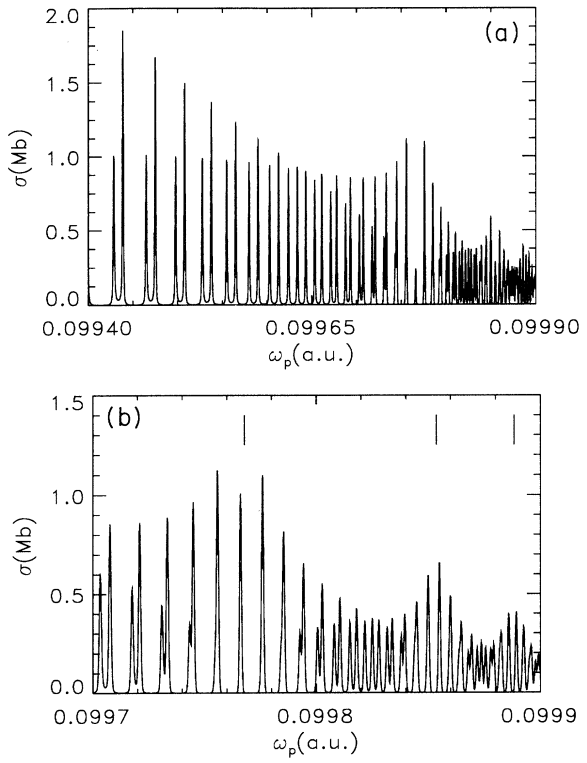

FIG. 3. (a) Cross section for absorption of a probe photon as a function of its frequency, ω_p. The resolution of the probe laser is taken to be 10^{-6} a.u. The driving laser is exactly on resonance and $d_{12}=10^{-5}$ a.u. (b) The vertical bars mark the energies where $\nu_1=\nu_2+k$ with $k=1,2,3$.

onance for any n. The glitches in Fig. 2 arise from accidental zero width resonances with $\nu_1=\nu_2+1$.

In Fig. 2 we show the evolution of the spectra with d_{12} when d_{12} is nearly equal to the resolution of the probe laser. In Fig. 3 we present the spectrum when $d_{12}=10^{-5}$ a.u. and the resolution of the probe laser is 10^{-6} a.u. at FWHM. In this figure we can clearly see the complex nature of this spectrum. Near 0.0994 a.u. the spectrum is fairly simple, consisting of two Rydberg series which can be unambiguously identified by their field-free quantum numbers. The series at slightly higher energy which has more of the oscillator strength can be identified with the bound-state series in zero field. The series at slightly lower energy can be identified with the $|P\rangle ns$ autoionizing series in zero field. Near 0.099 65 a.u. these two series become *strongly* mixed. This is the energy at which the classical frequency of the outer electron is twice the Rabi frequency. If the electron leaves the nucleus with the core in state $|S\rangle$, by the time it returns to the nucleus the core is in state $|P\rangle$ and vice versa.

In Fig. 3(b) we show the energy region with the complicated spectrum on an expanded energy scale. One striking feature of this graph is a periodicity in the "number" of Rydberg series visible in the spectrum with increasing n^*. Near $\omega_p=0.099\,77$ a.u., 0.099 85 a.u., and 0.099 89 a.u., the two Rydberg series merge into one within the assumed resolution of the probe laser. The three vertical bars in Fig. 3(b) mark the energies where a zero width resonance can appear, and in fact the resonances closest to these energies are extremely narrow and have not been theoretically resolved even though we have used 40 000 energy mesh points over the energy range shown in Fig. 3(b). The zero width resonances are at energies such that $\nu_1=\nu_2+k$ where $k=1,2,3\ldots$.

Another striking feature of these merged Rydberg levels is that the number of merged peaks is roughly the same (four, five, five) for each k. This fact can be understood from fairly simple scaling arguments. As long as $k\ll\nu_2$, the values for which $\nu_1=\nu_2+k$ are $\nu_2(k)\cong(k/d_{12})^{1/3}$. If the probe laser has a fixed resolution W, the fraction F of a Rydberg spacing at effective quantum number ν_2 which can be resolved is $F=sW\nu_2^3$ (when $F\simeq 1$, the Rydberg levels near effective quantum number ν_2 cannot be resolved). For each k, the fraction of a Rydberg spacing which can be resolved is $F(k)=sW\nu_2^3(k)=sWk/d_{12}$. As long as $|\nu_2+k-\nu_1|<F(k)$ the two Rydberg series will appear merged into one. This gives a lower value of ν_2 for which the series appears merged as $\nu_2\simeq(1-sW/d_{12})^{1/3}(k/d_{12})^{1/3}$ and an upper value of $\nu_2\simeq(1+sW/d_{12})^{1/3}(k/d_{12})^{1/3}$. Using $W/d_{12}=0.1$, $s=1.2$, and $d_{12}=10^{-5}$ a.u., this argument gives 3.7, 4.7, and 5.3 for the width in effective quantum number of the merged series. The two Rydberg series merged into one near $\nu_1=\nu_2+k$ because of the simple model which we chose. In general, the spectra near $\nu_1=\nu_2+k$ [where $|\nu_2+k-\nu_1|<F(k)$] will look like the spectra with the driving laser off.

In Fig. 4 we show the cross section for photoabsorption from two different ground states when the driving laser is tuned exactly to resonance and $d_{12}=8\times10^{-6}$ a.u. The lower curve is the same as in Fig. 2 with $d_{12}=8\times10^{-6}$ a.u. The upper curve is the photoabsorption cross section when the initial state has odd parity. For this case we choose $d_s^{(0)}=0$, and $d_p^{(+)}=1$ and $d_s^{(+)}=-1$. When the driving laser is off the probe laser

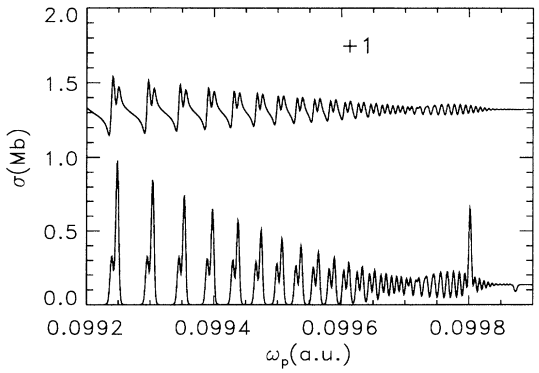

FIG. 4. Cross section for absorption of a probe photon as a function of its frequency, ω_p. The resolution of the probe laser is taken to be 5×10^{-6} a.u. The driving laser is exactly on resonance and $d_{12}=8\times10^{-5}$ a.u. The bottom curve is the same as in Fig. 2. The upper curve assumes the photoabsorption instead takes place from an excited state with dipole matrix elements $d_s^{(0)}=0$, $d_s^{(+)}=1$, and $d_p^{(+)}=1$.

excites the atom to the autoionizing region below the $|P\rangle$ state threshold. However, when the driving laser is turned on, it can de-excite the core state before the electron can return to the nucleus. In the nonperturbative region, two Rydberg series approaching the dressed thresholds are visible in the spectrum. This shows that the nonperturbative effects will be equally visible in spectra where the core state is excited or de-excited by the driving laser. For Fig. 4 we have again assumed the probe laser has a resolution of 5×10^{-6} a.u. ~1 cm^{-1}.

VI. REAL ATOMIC SYSTEM

In this section we show how to obtain the frame transformation matrix $\underline{U}$ for a general atomic system. We also show results for Mg when both lasers are linearly polarized in the same direction and the driving laser is resonant with either the $3s_{1/2}$-$3p_{1/2}$ transition or $3s_{1/2}$-$3p_{3/2}$ transition.

A. Frame transformation for Mg 3s-3p transitions

The specific atomic system which we will treat is the photoabsorption from the Mg $3s^2$ ground state when the driving laser is tuned to either the $3s_{1/2}$-$3p_{1/2}$ or the $3s_{1/2}$-$3p_{3/2}$ transition. The dynamics will be presented as a cross section for photoabsorption of a probe-laser photon as a function of the probe-laser frequency for a given frequency and intensity (represented by d_{12}) of the driving laser. The frequency ω_p of the probe-laser photon will be large enough to excite the Mg $3s^2$ ground state to a high Rydberg state $3snp$. Finally, the driving laser and the probe laser are taken to be linearly polarized in the same direction; this direction will be taken to be the direction of the z axis. Since the ground state has $J=0$ and the driving and probe lasers are linearly polarized in the z direction, only the $M=0$ states will play a role in the dynamics. Furthermore, only the odd-parity states with odd J at energy $E_g+\omega_p$ and the even-parity states with even J at energy $E_g+\omega_p+\omega_d$ will be coupled together because of the specific combination of polarization and ground-state angular momentum and symmetry of our problem [11]. The channels which we include in the calculation at energy $E_g+\omega_p$ of the undressed atomic system are $3s_{1/2}\varepsilon p_{1/2}$ and $3s_{1/2}\varepsilon p_{3/2}$ with $J=1$ and $3s_{1/2}\varepsilon f_{5/2}$ and $3s_{1/2}\varepsilon f_{7/2}$ with $J=3$. The channels which we include in the calculation at energy $E_g+\omega_p+\omega_d$ of the undressed atomic system are $3s_{1/2}\varepsilon s_{1/2}$, $3p_{1/2}\varepsilon p_{1/2}$, and $3p_{3/2}\varepsilon p_{3/2}$ with $J=0$, and $3s_{1/2}\varepsilon d_{3/2}$, $3s_{1/2}\varepsilon d_{5/2}$, $3p_{1/2}\varepsilon p_{3/2}$, $3p_{3/2}\varepsilon p_{1/2}$, $3p_{3/2}\varepsilon p_{3/2}$, $3p_{1/2}\varepsilon f_{5/2}$, $3p_{3/2}\varepsilon f_{5/2}$, and $3p_{3/2}\varepsilon f_{7/2}$ with $J=2$, and $3s_{1/2}\varepsilon g_{7/2}$, $3s_{1/2}\varepsilon g_{9/2}$, $3p_{1/2}\varepsilon f_{7/2}$, $3p_{3/2}\varepsilon f_{5/2}$, and $3p_{3/2}\varepsilon f_{7/2}$ with $J=4$. Of course all of the channels have $M=0$.

The frame transformation for a real atom is only slightly more complicated than that discussed for the model problem of Sec. III B. The only difficulty is that for the undressed atom the total angular momentum of the core is coupled to the total angular momentum of the outer electron to give the total angular momentum of the atom and its projection along the z axis. However, this difficulty is easily overcome by applying a frame transformation which decouples the two angular momenta,

$$K_{ij_cm_cj_0m_0,i'j_c'm_c'j_0'm_0'} = \sum_{J,M}(j_cm_cj_0m_0|JM)K^J_{j_cj_0,j_c'j_0'}(JM|j_c'm_c'j_0'm_0'), \quad (27)$$

where K^J is the atomic, jj-coupled K matrix and $(j_cm_cj_0m_0|JM)=(JM|j_cm_cj_0m_0)$ is the Clebsch-Gordan coefficient as defined in Edmonds [12]. The dipole matrix element in this frame is

$$d_{ij_cm_cj_0m_0}=\sum_{J,M}d^{JM}_{ij_cj_0}(JM|j_cm_cj_0m_0). \quad (28)$$

The driving laser causes transitions between some of the core states; this channel mixing is handled in the same way as the model problem,

$$K_{\alpha\mu j_0m_0,\alpha'\mu'j_0'm_0'} = \sum_{i,j_c,m_c,i',j_c',m_c'}(U^\dagger)_{\alpha\mu,ij_cm_c} \times K_{ij_cm_cj_0m_0,i'j_c'm_c'j_0'm_0'}U_{i'j_c'm_c',\alpha',\mu'}. \quad (29)$$

The dipole matrix element is

$$d_{\alpha\mu j_0m_0}=\sum_{i,j_c,m_c}d_{ij_cm_cj_0m_0}U_{ij_cm_c,\alpha\mu}. \quad (30)$$

Equations (27)–(30) show the full frame transformation for a general dressed channel atom. However, it is not always necessary to use these general equations because the final reaction matrix, Eq. (29), will often have a "simple" block-diagonal form. For example, for the Mg example discussed in this section, we were able to obtain the full; frame transformation matrix by listing all of the relevant channels and inspecting their angular couplings.

B. Results

In Figs. 5–7 we show our calculated cross sections when the driving laser is tuned to the $3s_{1/2}$-$3p_{1/2}$ transition to Mg. In all of these figures the driving laser is exactly on resonance. These figures show how the spectrum evolves for several values of d_{12} and the resolution of the

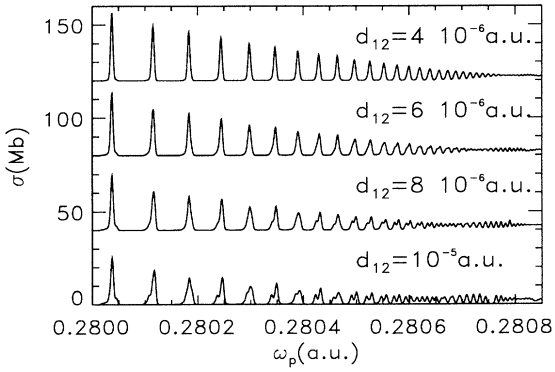

FIG. 5. Same as Fig. 2 except for Mg with the driving laser exactly on resonance with the $3s_{1/2}$-$3p_{1/2}$ transition in Mg^+.

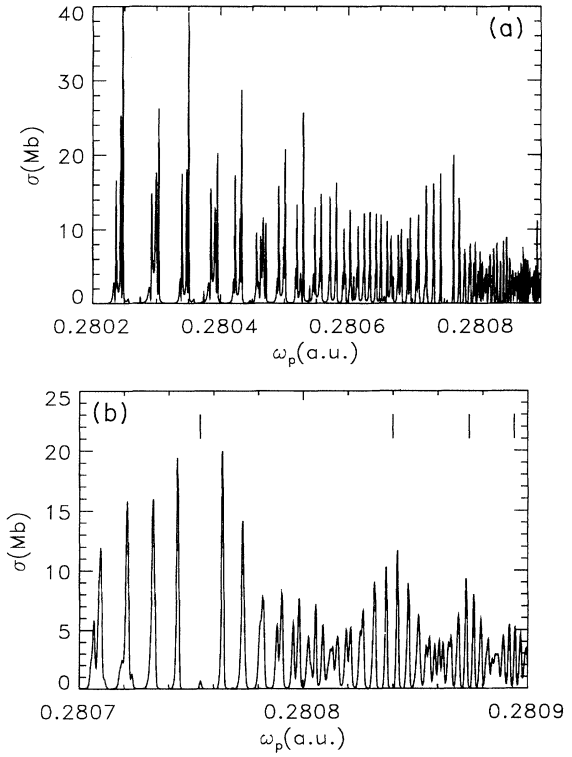

FIG. 6. Same as Fig. 2 except for Mg with the driving laser exactly on resonance with the $3s_{1/2}$-$3p_{1/2}$ transition in Mg^+.

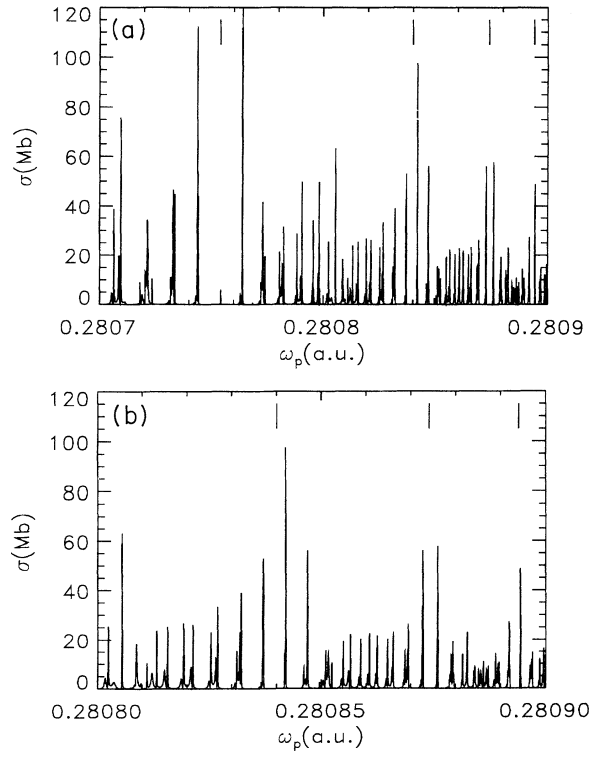

FIG. 7. Same as Fig. 6 except with a probe-laser resolution 10^{-7} a.u. FWHM.

probe laser. The ratio of d_{12} divided by the resolution is probably the most important parameter which determines the appearance of the spectrum. When this ratio is less than one, the spectrum looks like a simple unperturbed Rydberg series approaching the $3s_{1/2}$ threshold. As this ratio becomes larger, the spectrum becomes increasingly complex. Probably one of the more striking features of these figures is the similarity between some of the Mg spectra and the corresponding model problem spectra of Sec. V.

In Fig. 5 we show the cross section for absorption of a probe photon as a function of the probe-laser frequency for several different values of d_{12} which are nearly equal to the resolution of the probe laser. We have assumed the probe laser has a resolution of 5×10^{-6} a.u. ~1 cm^{-1} FWHM. This figure should be compared to Fig. 2. The similarity between these two figures is remarkable. Remember that the model problem which generated Fig. 2 had two Rydberg series approaching the Rabi split thresholds and one open channel while Mg has eight Rydberg series approaching the Rabi split thresholds as well as hundreds of perturbing states which are attached to the $3p_{3/2}$ threshold. In Sec. V we say that the nonperturbative effects become visible for $d_{12}=(8-10)\times10^{-6}$ a.u. because both Rydberg series are clearly visible as well as strongly interacting. However, because Fig. 5 resembles Fig. 2 so closely, it is safe to say that these nonperturbative effects are a generic characteristic of the Rabi splitting and the resolution and do not depend strongly on the atomic dynamics.

In Fig. 6 we show the cross section when the assumed probe-laser resolution is 10^{-6} a.u. FWHM and $d_{12}=10^{-5}$ a.u. These figures should be compared to Fig. 3 for the model problem. At this combination of resolution and Rabi splitting the complex underlying dynamics of Mg is clearly visible near 0.2803 a.u. in Fig. 6(a). The complex appearance of the resonances near this energy is due to the interaction induced by the driving laser as well as perturbations from the Rydberg states attached to the $3p_{3/2}$ threshold. It is pointless at this time to name each of these structures because the spectrum is specific to our chosen atomic system and excitation scheme. Suffice it to say that when the Rabi splitting of the thresholds is a factor of 10 or larger than the resolution, the spectrum becomes dependent on the specific atom or molecule used in the experiment. In Fig. 6(b) we show the spectrum on an expanded energy scale which should be compared to Fig. 3(b) for the model problem. Again we see regions of remarkable simplicity in a region where the spectrum "should" be very complex. On this figure, we have again marked the energies where $\nu_1=\nu_2+k$ ($k=1,2,3,4$) with vertical bars. These are the energies where there is a possibility of zero width resonances. In fact, the resonance at $\sim0.280\,75$ a.u. has a very small theoretical width; we used 60 000 energy mesh points to cover the energy range of Fig. 6(b) and this resonance is still unresolved (because it is unresolved it appears to have an anomalously small oscillator strength). Physically, the vertical bars mark the energies where the excited electron is just returning to the nucleus when the driving laser has just finished exciting and de-exciting the core once (for $k=1$), twice (for

$k=2$), etc. Since the outer electron is returning to the nucleus when the core is exactly the same state as when the outer electron left, the dynamics is identical to that with the driving laser turned off. Therefore, the spectrum appears to be simple at these energies.

In Fig. 7 we show the cross section when the assumed probe-laser resolution is 10^{-7} a.u. FWHM and $d_{12}=10^{-5}$ a.u. At this higher resolution, the simple spectrum of Fig. 6(b) becomes complex. However, there are still some islands of simplicity near $\nu_1=\nu_2+k$ (which are marked by vertical bars on the graph) although these islands are smaller than in Fig. 6(b) because of the higher resolution. Again some of the resonances have a very complex structure which we have not tried to classify. In Fig. 7(b) there appears to be possibly other islands of simplicity around the energies $\nu_1=\nu_2+k+\frac{1}{2}$. At these energies, if the electron leaves the core in the $3s_{1/2}$ state, it returns when the core is in the $3p_{1/2}$ state and vice versa (i.e., the second time the electron returns to the nucleus the core is in the same state as when the electron originally left).

In Fig. 8 we show the cross section when the driving laser is exactly on resonance with the $3s_{1/2}$-$3p_{3/2}$ transition. The assumed probe-laser resolution is 10^{-7} a.u. FWHM and $d_{12}=10^{-5}$ a.u. These figures should be compared with Fig. 7 for the $3s_{1/2}$-$3p_{1/2}$ transition. Notice that the spectra are nearly identical when $\nu_1=\nu_2+k$ as expected. The differing atomic dynamics is only apparent for the energies near $\nu_1=\nu_2+k+\frac{1}{2}$.

Finally, there is one last factor which may affect the observability of the phenomenon which we have discussed in this paper. Namely, the positions of the resonances depends on d_{12} and therefore if d_{12} changes from measurement to measurement or even during a particular measurement, the resonances could become smeared out. In Fig. 9 we try to model this effect by averaging the cross sections with $d_{12}=9$, 10, and 11×10^{-6} a.u. for a probe laser with a resolution of 10^{-7} a.u. FWHM. The coefficients which we have used for the averaging are $\frac{1}{4}$, $\frac{1}{2}$, and $\frac{1}{4}$ [i.e., in Fig. 9 we plot the "averaged" cross section, $\sigma=\sigma_9/4+\sigma_{10}/2+\sigma_{11}/4$]. In Fig. 9 the spectra are definitely smeared out compared to those in Fig. 8. The resonances near the energies $\nu_1=\nu_2+k$ with $k=1,2,3,4$ (which are marked by the vertical bars in the figures) in Fig. 9 have broadened compared to those in Fig. 8 but they still seem to be distinct. However, at the energies near $\nu_1=\nu_2+k-\frac{1}{2}$ (which are about halfway between adjacent vertical bars) the spectra are very smeared out due to the higher density of resonances at these energies. Fluctuations in d_{12} definitely lead to a smearing of the spectra. As a rule of thumb, the smearing will be of the same size as the "fluctuations" in d_{12}. For example, if the resolution of the probe laser is 10^{-8} a.u. and d_{12} can change by 10^{-7} a.u. from measurement to measurement, the apparent resolution will be close to 10^{-7} a.u. As another example, if the resolution of the probe laser is 10^{-8} a.u. and d_{12} can change by 10^{-9} a.u. the apparent resolution will be close to 10^{-8} a.u. This analysis shows that it will be crucial to keep d_{12} as consistent as is exper-

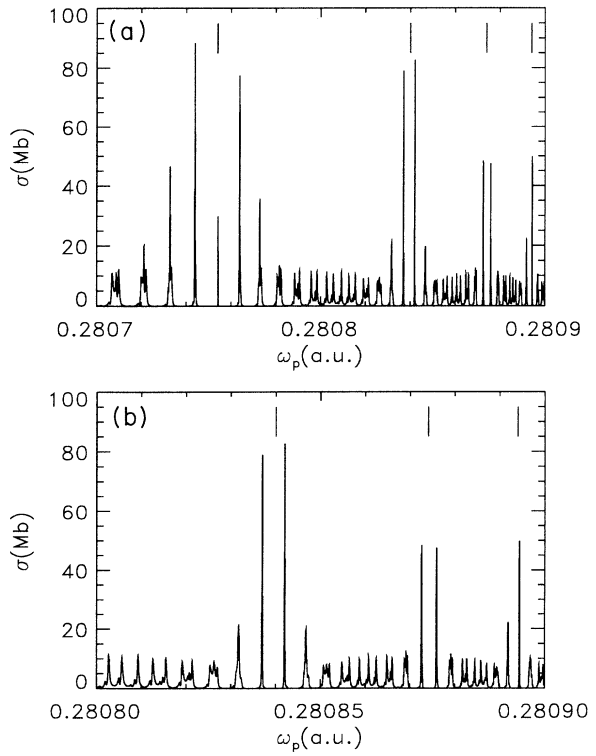

FIG. 8. Same as Fig. 7 except with the driving laser resonant with the Mg^+ $3s_{1/2}$-$3p_{3/2}$ transition.

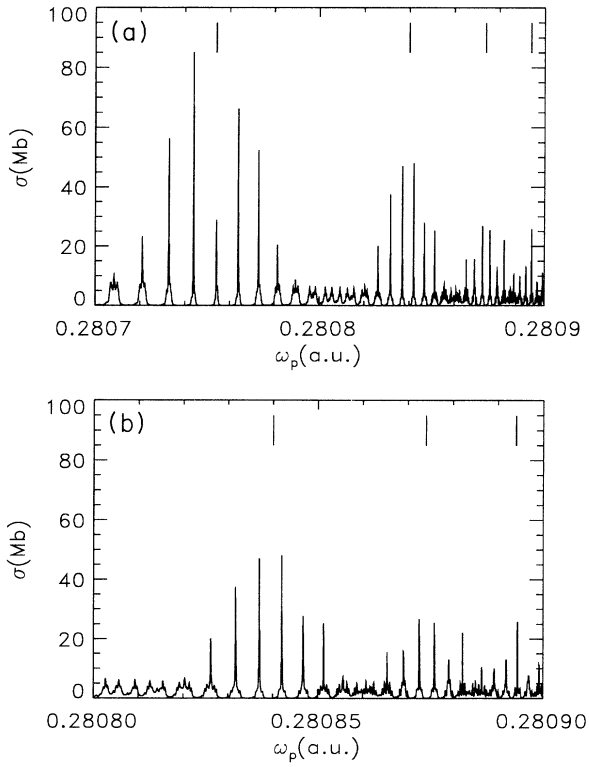

FIG. 9. Same as Fig. 8 except we have averaged the cross sections with $d_{12}=9$, 10, and 11×10^{-6} a.u. with coefficients $\frac{1}{4}$, $\frac{1}{2}$, and $\frac{1}{4}$.

imentally possible to avoid having the effect washed out.

At this point, we would like to repeat some of the main ideas in this section. When the Rabi frequency is slightly larger than the resolution, the spectrum does not depend very much on the atomic dynamics. The amount of complexity in the spectrum depends crucially on the Rabi frequency compared to the resolution. Many of the resonances are weak and/or closely spaced. It seems that the full complexity of the atom-laser dynamics starts to become apparent when the Rabi frequency is a factor of 100 or more larger than the resolution. However, striking nonperturbative effects are apparent at much smaller Rabi frequencies (e.g., when the Rabi frequency is only a factor of 10 larger than the resolution).

VII. CONCLUSIONS

In this paper we have presented the formalism necessary to theoretically describe the atomic dynamics when two core states of an atom are strongly coupled by a resonant laser field. We use a frame transformation to obtain the scattering parameters for the dressed channels in terms of scattering parameters of the undressed channels. In this approximation we are completely ignoring the interaction of the driving laser with the outer electron; we also ignore the interaction of the atom with the driving laser when *all* of the electrons are near the nucleus. The interaction we are ignoring gives above threshold ionization; we are confident that our method will work when there is very little above threshold ionization.

We have described a type of experiment which should be able to detect nonperturbative effects due to the Rabi oscillation of the core states. It seems that the sole requirement for detecting these effects is that the Rabi frequency of the driven core states must be larger than the total resolution of a probe-laser–atom system. By total resolution, we mean the broadening due to the laser, the doppler effect, scattering, etc. When the Rabi frequency is greater than twice the experimental resolution, Rydberg series converging to each of the dressed state thresholds become clearly visible in the spectra.

We have calculated the spectra which results from a simple model problem in order to get a feel for the basic effects. From this calculation we see that striking effects occur both when the driving laser excites the core and also when it deexcites the core. The driving laser needs to couple two states in which one of the states is a part of an important channel in the undressed atomic dynamics. For example, in Ca the driving laser can be tuned to any of the $4s_{1/2}$-$4p_J$ transitions, or $3d_J$-$4p_{J'}$, or $3d_J$-$4f_{J'}$ transitions. We have also calculated the ionization spectra for Mg as a function of the frequency of the probe laser when the driving laser is tuned to the $3s_{1/2}$-$3p_{1/2}$ transition as well as the $3s_{1/2}$-$3p_{3/2}$ transition. The probe laser has enough energy to excite Mg from its $3s^2$ ground state to high-lying Rydberg states, $3s_{1/2}np_j$, just below the $3s_{1/2}$ threshold. This system is probably not experimentally accessible due to the high-frequency photons which are needed for the excitations; however, these calculations for a real, multichannel atom give an idea of what to expect experimentally for given combinations of Rabi frequency and resolution. It is impossible that the most accessible systems experimentally will be the heavier atoms, for which substantial intensity in the lower-frequency driving laser can be obtained.

ACKNOWLEDGMENTS

I thank D. Armstrong for useful discussions about experimental aspects of this problem and C. H. Greene, P. Zoller, and Bo Gao for useful discussions about theoretical aspects of this problem. I also thank P. Zoller for suggesting this problem. This research is supported by the Division of Chemical Sciences, Office of Basic Energy Sciences, Office of Energy Research, U.S. Department of Energy Grant No. DE-FG-02-90ER14145.

[1] K. Kulander, Phys. Rev. A **36**, 2726 (1987); X. Tang, H. Rudolph, and P. Lambropoulos, *ibid.* **44**, 6994 (1991).

[2] Th. Mercouris and C. A. Nicolaides, J. Phys. B **21**, L285 (1988); M. Dörr, R. M. Potvliege, D. Proulx, and R. Shakeshaft, Phys. Rev. A **42**, 4138 (1990).

[3] (a) W. E. Cooke, T. F. Gallagher, S. A. Edelstein, and R. M. Hill, Phys. Rev. Lett. **40**, 178 (1978); (b) G. W. Schinn, C.-J. Dai, and T. F. Gallagher, Phys. Rev. A **43**, 2316 (1991); (c) M. D. Lindsay, C.-J. Dai, L.-T. Cai, T. F. Gallagher, F. Robicheaux, and C. H. Greene, *ibid.* **46**, 3789 (1992).

[4] U. Fano and A. R. P. Rau, *Atomic Collisions and Spectra* (Academic, Orlando, FL, 1986); M. J. Seaton, Rep. Prog. Phys. **46**, 167 (1983).

[5] For example, see *Atomic Spectra and Collisions in External Fields,* edited by K. T. Taylor, M. H. Nayfeh, and C. W. Clark (Plenum, New York, 1988).

[6] A. Giusti-Suzor and P. Zoller, Phys. Rev. A **36**, 5178 (1987).

[7] P. S. Julienne, Phys. Rev. Lett. **61**, 698 (1988); P. S. Julienne and R. Heather, *ibid.* **67**, 2135 (1991); P. D Lett, P. S. Jessen, W. D. Phillips, S. L. Rolston, C. I. Westbrook, and P. L. Gould, *ibid.* **67**, 2139 (1991).

[8] U. Fano, Phys. Rev. A **2**, 353 (1970); C. M. Lee and K. T. Lu, *ibid.* **8**, 1241 (1973); U. Fano, J. Opt. Soc. Am. **65**, 979 (1975).

[9] W. E. Cooke and C. L. Cromer, Phys. Rev. A **32**, 2725 (1985).

[10] Q. Wang and C. H. Greene, Phys. Rev. A **44**, 1874 (1991).

[11] All of the field-free atomic (MQDT) parameters were calculated by C. H. Greene (unpublished).

[12] A. R. Edmonds, *Angular Momentum in Quantum Mechanics* (Princeton University Press, Princeton, NJ, 1974).